JOTCS A
Journal of the Turkish Chemical Society
Section: A
Chemistry

TURKISH CHEMICAL SOCIETY

Investigation of Adsorptive Removal of Methylene Blue from Synthetic Wastewater Using Polymeric Composite

Monsuru Dauda[1,2], Ayobami Ajani[1,2], Abass Alade[1,2,3*], Tinuade Jolaade Afolabi[1,2]

[1]Ladoke Akintola University of Technology, Department of Chemical Engineering, Faculty of Engineering, Ogbomoso, Nigeria.
[2]Ladoke Akintola University of Technology, Bioenvironmental, Water and Engineering Research Group (BWERG), Ogbomoso, Nigeria.
[3]Ladoke Akintola University of Technology, Science and Engineering Research Group (SAERG), Ogbomoso, Nigeria.

Abstract: Recycling polymeric waste into another useful material is considered to be the preferred way of taking care of the issues of slow degradable plastic waste, particularly in anticipation of natural contamination. In this study, the adsorptive treatment of Methylene Blue (MB) using adsorbents from chemically recycled polymeric waste was investigated. Three polymeric materials were employed in this study: styrofoam waste (EPS1), intruded extended polystyrene (EPS2), and sunflower xylem (*Tithonia diversifolia* xylem) (TDX). The alterations in microscopic surface morphology before and after the adsorption process were examined using scanning electron microscopy (SEM) system to resolve the intercalation of MB with the adsorbent. The experimental batch data was collected and the effects of concentration and contact time on the removal of MB from synthetic wastewater were studied. Adsorption kinetics, equilibrium, and thermodynamics were studied and fitted by various models. According to the result, the uptake of adsorbate increased as contact time and concentration rose, with the pseudo-second-order model best depicting the adsorption kinetics.

Keywords: Adsorbent composite; Methylene blue; Polymeric adsorbents.

Submitted: July 26, 2022. **Accepted:** August 3, 2023.

Cite this: Dauda M, Ajani A, Alade A, Afolabi TJ. Investigation of Adsorptive Removal of Methylene Blue from Synthetic Wastewater Using Polymeric Composite. JOTCSA. 2023;10(4):961-74.

DOI: https://doi.org/10.18596/jotcsa.1148910

***Corresponding author's E-mail:** aoalade@lautech.edu.ng

1. INTRODUCTION

The new lifestyle has pushed humanity towards the massive use of plastic materials for most edible, medical, and other personal care products (1). Tragically, the treatment of plastic waste is not remote from the expanded interest in plastic items. A basic and notable method for curing polymeric waste is burning, however, it creates potentially perilous discharges. In this manner, reusing is viewed as the preferred approach to tackling the issues of slow degradable plastic waste, particularly in anticipation of natural contamination. Notwithstanding, the interaction is expensive since the cost of the hydrocarbon and monomer is a lot lower than that recuperated by recycling (1). Thus, significant consideration has been paid to the compound reusing of polymeric waste to yield different valuable materials like adsorbents (1, 2).

Polymeric adsorbents can trap a large number of the omnipresent organic contaminants, in particular colors, phenolic compounds, natural acids, fragrant or polyaromatic hydrocarbons, alkanes, and their derivatives. Polymeric materials appear to be more appealing than activated carbon, cellulose, alginate, diatomite, and sand, because of their superb mechanical strength and movable surface chemistry (2). These polymers as adsorbents display the following properties: vast surface area and wonderful skeleton strength, basic physicochemical properties like internal surface region and pore size dissemination that can be adjusted by fluctuating the polymerization conditions, high water

sanitization limit, colorless, scentless, and non-harmful, low expense, re-expanding limit, biodegradability, biocompatibility, good toughness, and stability in a swelling environment (3).

Removal of MB from industrial wastewater has been explored utilizing different techniques, for example, sedimentation, nanofiltration, filtration innovation, synthetic treatment with coagulating flocculating materials, oxidation by utilizing oxidizing agents, electrochemical techniques, high-level oxidation processes (AOPs), enzymatic interaction, photodegradation response, electrochemical evacuation, chemical coagulation, film filtration, and physical adsorption methods (4,5). Among them, the adsorption process is among the most researched methods for MB removal, and it has ended up being effective and economical in the removal of refractory pollutants (including dye) from wastewater due to its lower initial development cost, simple design, easy operation, and free from or less generation of poisonous substances (6).

2. MATERIALS AND METHODS

2.1. Sampling and Preparation of Polymeric Composite

Samples of polymeric materials, which are Styrofoam waste (EPS1), intruded extended polystyrene (EPS2), and "*Tithonia diversifolia xylem"* (TDX*),* were used. The samples were washed to remove the oil, dust, and sand particles from them. Washed materials were sun-dried till the materials became very dry and then underwent surface area reduction using milling processes at 8000 rpm. Phosphoric acid, H_3PO_4 (Aldrich) (3 M) was used for chemical activation for 24 h. The adsorbents were neutralized to a pH range of 6.9 - 7.1 with sodium hydroxide (NaOH) (BDH), filtered immediately, and dried very well (7).

2.2. Preparation of Adsorbate Solution

Methylene Blue ($C_{16}H_{18}N_3SCl$, BDH) was bought from Bond Chemicals, Ibadan, Oyo State. Methylene blue was used without further purification and was prepared with distilled water. A stock solution of 1000 mg/L was first prepared by dissolving 1.127 g of methylene blue in 1000 mL of distilled water. The experimental solution (50 mg/L) was prepared by diluting the stock solution with distilled water. The concentration of MB was then determined at 665 nm by a UV–visible spectrophotometer.

2.3. Characterization of the Adsorbent

The structural chemical functional groups of the adsorbents were determined utilizing the Fourier Transform Infrared Technique (FTIR, Nicolet IS5) and the before and after adsorption microscopic surface morphology changes of samples were determined using SEM images obtained using the scanning electron microscopy (SEM) system. The working voltage choice was within the scope of 10-20 kV (8).

2.4. Batch Adsorption Studies

A batch adsorption experiment was done to evaluate the adsorption behavior of the adsorbent. The MB parameters of concentration of adsorbate, contact time, and adsorbent dosage were studied. A solution (100 mL) of different concentrations from 40-100 mg/L was brought into contact with 1 g of the optimized polymeric composite adsorbent at a different time (10-110 min) to determine the effect of contact time and change in concentration. The adsorption capacity and removal efficiency were evaluated in Equations 1 and 2, respectively. The data obtained were used to estimate equilibrium relationships between sorbent and adsorbate at a constant temperature using adsorption isotherm techniques. Adsorption kinetics were also estimated to describe the rate of retention or release of MB from simulated waste water to a solid-phase polymeric adsorbent interface.

2.5. Optimization of Contact Time

The 100 mg/L prepared solution of MB was diluted with water to obtain 80 mg/L, 60 mg/L, 50 mg/L, and 40 mg/L. Polymeric adsorbent (1 g) composite with the optimized ratio of 20% of material Styrofoam to 20% of material intruded EPS to 60% of material TDS and 100 mL of each solution of MB synthesized wastewater into eleven different flasks of 250 mL capacity, varying contact time between 10 and 110 min. All the flasks were placed in a rotary shaker at 180 rpm. Then, flasks were withdrawn from the shaker in the range of 10–110 min, respectively, to optimize and relate the activeness of the adsorbent to the time, after keeping the rate of agitation and temperature constant. A plot of MB q_e against time was used to optimize time for further study and a plot of MB removal against time was utilized to examine the contact time for the adsorption process.

2.6. Initial MB Concentration and Adsorption Capacity

MB solutions (100 mL) of concentrations between 40 and 100 mg/L each were placed into different flasks of 250 mL capacity and equilibrated with 1 g of the polymeric adsorbent composite with the optimized ratio of 20% of material Styrofoam, 20% of material Intruded EPS and 60% of material TDS. All the flasks were placed in a rotary shaker at 180 rpm. Then, flasks were withdrawn from the shaker at a constant time to relate the activeness of the adsorbent to the adsorbate concentration after keeping the rate of agitation and temperature constant. The data obtained were fitted to adsorption isotherm models.

2.7. Calculations

2.7.1. Uptake and adsorption removal

The MB uptake per gram of sorbent and the percentage of adsorption removal were calculated using Equations 1 and 2:

$$q_e = \frac{C_O - C_e}{m} V \quad (1)$$

$$\%RE = \frac{C_O - C_e}{C_O} * 100\% \quad (2)$$

where m is the mass of the composite (g). q_e was the equilibrium adsorption capacity (mg/g), C_0 is the initial MB concentration (mg/L), C_e is the experimental concentration (mg/L) of MB solution, V was the volume of aqueous solution (L) and m was the dry weight of the adsorbent (g).

2.7.2. Langmuir isotherm model

The adsorption isotherm inferred by Langmuir for the adsorption of a solute from a fluid arrangement is given in Equation 3 (9).

$$q_e = \frac{q_m K_a C_e}{1 + K_a C_e} \quad (3)$$

where q_e is the amount of adsorbate adsorbed per unit amount of adsorbent at equilibrium (g/mg), q_m is *the a*mount of adsorbate adsorbed per unit amount of adsorbent required for monolayer adsorption (limiting adsorbing capacity), K_a is the constant related to enthalpy of adsorption $(L/\mu g)^n$, and C_e is the concentration of adsorbate solution at equilibrium (mg/L). The four linear forms of the Langmuir isotherm model considered are given in Equations 4-7.

2.7.3. Langmuir first isotherm model

$$\frac{C_e}{q_e} = \frac{1}{q_m K_a} + \frac{1}{q_m} C_e \quad (4)$$

Using a linear mathematical expression for the Langmuir model, a graph can be obtained by plotting C_e / q_e Vs C_e.

2.7.4. Langmuir second isotherm model

$$\frac{1}{q_e} = \frac{1}{q_m} + \frac{1}{k_a q_m C_e} \quad (5)$$

A plot of 1 / q_e against 1 / C_e gives an intercept of 1 / q_m and a slope of 1 / $k_a q_m$ (10).

2.7.5. Langmuir third isotherm model

$$q_e = q_m - \frac{q_e}{k_a C_e} \quad (6)$$

A plot of q_e against q_e / C_e gives an intercept of q_m and a slope of -1 / K_a (10).

2.7.6. Langmuir fourth isotherm model

$$\frac{q_e}{C_e} = K_a q_m - q_e \quad (7)$$

A plot of q_e / C_e against q_e gives an intercept of $K_a q_m$ and a slope of K_a (10). (11) introduced a dimensionless equilibrium term **R,** otherwise called the partition component to communicate the Langmuir consistency b. The essential characteristic of the Langmuir isotherm can be expressed in terms of dimensionless constant separation factor R_L (7). Langmuir isotherm is often investigated with dimensionless separation factor **R** according to Equation 8 (7)

$$R = \frac{1}{1 + K C_0} \quad (8)$$

where C_0 is the initial concentration of adsorbate (mg/L) and K_L is Langmuir constant.

The value of the dimensionless separation factor **R** gives significant data about the idea of adsorption. The value of **R** is somewhere in the range of 0 and 1 for good adsorption, while **R**>1 addresses negative adsorption and **R** = 1 addresses linear adsorption. The adsorption interaction is irreversible if **R** = 0 (12).

2.7.7. Freundlich Isotherm model

The Freundlich model (13) is an empirical equation and may be the most broadly utilized nonlinear sorption model since it precisely depicts a lot of adsorption information for heterogeneous adsorbent surfaces. The model is introduced as Equation 9, while the linearized form can be represented as Equation 10:

$$qe = K C_e^{1/n} \quad (9)$$

$$\log qe = \log K + \frac{1}{n} \log C_e \quad (10)$$

where q_e is the MB uptake (mg/g) at equilibrium, K is the proportion of the sorption limit, 1/n is the sorption intensity, and C_e is the equilibrium concentration ($mg.L^{-1}$). K_f and n are Freundlich constants connected with the adsorption capacity and adsorption force, respectively. These boundaries can be determined from the capture and the slope of the linear plot of log q_e against log C_e. The slope, which ranges between 0 and 1 is a measure of adsorption force or surface heterogeneity, becoming more heterogeneous as its value gets closer to zero.

2.7.8. Temkin isotherm model

Temkin studied the adsorbate-adsorbate interactions in an adsorption process and the model is introduced as Equation 11, while the linear form is represented as Equation 12:

$$q_e = \frac{RT}{\Delta q} \in K_O + \frac{RT}{\Delta q} \in C_e \quad (11)$$

$$q = BInA + Bln\,C_e \quad (12)$$

Where B = RT / Δq, T is the absolute temperature in K and R is the universal gas constant of 8.3143 J/mol K. The steady is connected with the intensity of adsorption q_e (mg/g) and C_e (mg/L) and the equilibrium concentration, respectively. A and B are constants connected with the adsorption limit and force of adsorption. A plot of q_e versus lnC_e yields a slope of B and an intercept of Blna (14).

2.7.9. Harkin – Jura isotherm model

The Harkin-Jura isotherm model portrays the chance of multi-facet adsorption on the outer layer of the adsorbent having heterogeneous pore dissemination as illustrated in Equation 13:

$$\frac{1}{q_e^2} = \frac{B}{A} - \frac{1}{A}\log C_e \quad (13)$$

Where A and B are Harkin-Jura constants that can be gotten by plotting 1 / q_e^2 against logC_e (14).

2.7.10. Hill-De Boer isotherm model

Hill-De Boer isotherm model portrays a situation where there is versatile adsorption as well as horizontal interaction among adsorbed particles. The linearized type of this isotherm model is expressed as follows (Equation 14):

$$\ln\left(\frac{C_e^2}{C_o - C_e}\right) - \frac{C_o - C_e}{Ce} = -\ln K_1 - \frac{K_2(C_o - C_e)}{RT\,.\,C_o} \quad (14)$$

Where K_1 and K_2 are the Hill-DeBoer constant in (L/mg) and the constant of the interaction between adsorbed molecules (KJ/mol) respectively. Experimental data from the adsorption process can be analyzed by plotting $\ln\left(\frac{Ce^2}{C_o - C_e}\right) - \frac{C_o - C_e}{C_e}$ against $\frac{C_o - C_e}{C_o}$, where the slope is $\frac{-K_2}{RT}$ and the intercept is -lnK_1 (14).

2.7.11. Dubinin–Radushkevich isotherm (D-R) model

Dubinin-Radushkevich isotherm model is an adsorption model that is applied to impart the adsorption instrument with Gaussian energy dispersion onto heterogeneous surfaces. This isotherm is only fitting for an intermediate range of adsorbate focuses because it shows an absurd asymptotic way of behaving and doesn't predict Henry's laws at low pressure. It is expressed numerically as (Equation 15):

$$q = q_e e^{-\beta RT \ln\left(1 + \frac{1}{C_e}\right)^2} \quad (15)$$

where, q = maximum adsorption capacity (mg/g), q_e = equilibrium adsorption capacity (mg/g), β = Free energy of adsorption per mole of adsorbate, C_e = equilibrium concentration (mg/L).

The Dubinin-Radushkevich isotherm model is expressed in linear logarithmic form (Equation 16)

$$\ln q_e = \ln q - \beta\varepsilon^2 \quad (16)$$

ε =Polanyi potential which is given as (Equation 17)

$$\varepsilon = RTIn\left(1 + \frac{1}{C_e}\right) \quad (17)$$

where R is the gas constant (8.34 J/mol/K) and T is the absolute temperature. A plot of ln q_e versus ε^2 gives the slope β and intercept ln q_e (14).

2.7.12. Jovanovich isotherm model

Assumptions contained in the Langmuir model were used in predicting the Jovanovich model, but in adding the possibility of some mechanical contact between the adsorbent and adsorbate (14). The linear form of the Jovanovich isotherm is expressed as (Equation 18):

$$\ln q_e = \ln q_{max} - K_f C_e \quad (18)$$

Where q_e is the amount of adsorbate in the adsorbent at equilibrium (mg/g), q_{max} is the maximum uptake of adsorbate (L/mg). The plot of ln q_e against C_e gives a straight line, and Jovanovich constants K_f and q_{max} were evaluated using the slope and intercept of the plot, respectively (14).

2.8. Sorption Kinetics

2.8.1. Zeroth order kinetics

A Zeroth Order Kinetics equation is given as (Equation 19):

$$q_t^* = q_o^* + K_o t \quad (19)$$

Where q_t^* is the amount of solute sorbed on the surface of the sorbent at any time, t, (mg/g), q_o^* is the amount of solute sorbed at time t = 0 (mg/g), and K_o zero-order reaction rate constant, (mg/g min). A plot of q_t^* against t gives a straight line, and K_o and q_o^* can be calculated using the slope and intercept, respectively (10).

2.8.2. First-order model

The first-order condition for sorption in the fluid system depends on the solid limit. The Lagergren rate condition is the most generally involved rate condition for the sorption of a solute from a fluid arrangement (Equation 20).

$$\frac{dq_t}{dt} = K_1(q_m - q_t) \quad (20)$$

Integrating this for the initial (t = 0 and q_t = 0) and end conditions (t = t and q_t = q_t), Equation (21) may be rearranged for linearized data plotting as shown by Equation (22):

$$\log(q_m - q_t) = \log q_m - \frac{k_1}{2.303}t \quad (21)$$

Equation (21) is applied and the parameter q_m is evaluated, using experimental data. The boundary q_m does not address the quantity of accessible sites. The boundary log (q_m) is a movable boundary, and it's rarely equivalent to the intercept of a plot of log (q_m-q_t) against t, while, in a genuine first-order system, log (q_m) ought to be equivalent to the intercept of a plot of log (q_m-q_t) against t. Equation (22) is only an approximate solution to the first-order rate mechanism (10).

2.8.3. Pseudo-first-order model (PFO)

A pseudo-first-order kinetic model equation is given as Equation 22 (15):

$$\ln\left(q_e - q_t\right) = \ln q_e - k_1 t \quad (22)$$

Where q_e is the adsorption capacity at equilibrium (mg/g), q_t is the amount of pollutant removed at time t (mg/g), k_1 is the pseudo-first-order rate constant (1/min), and t is the contact time (min) (10).

2.8.4. Second-order model

A second-order kinetic model is given as Equation 23;

$$\frac{1}{q_t} = \frac{1}{q_0} + K_2 t \quad (23)$$

Where q_t is the amount of pollutant removed at time t (mg/g), q_o is the amount of solute sorbed at time t = 0 (mg/g), and K_2 second-order rate constant (g/mg min). The plot of 1 / q_t against t gives a straight line and the values for K_2 and q_o can be calculated from the slope and intercept, respectively (10).

2.8.5. Pseudo-second-order model (PSO)

The pseudo-second-order model is expressed in Equation 24 and its linear form is given in Equation 25.

$$\frac{d_q}{d_t} = k_2 \quad (24)$$

$$\frac{t}{q_t} = \frac{1}{k_2 q_e^2} + \frac{t}{q_e} \quad (25)$$

Where, k_2 (mg/g/min), t and q_e are the pseudo-second-order rate constant, time, and adsorption capacity at equilibrium, respectively. They were determined from the plot of t / q_t versus t (10).

2.8.6. Third-order model

The third-order kinetic equation is given as:

$$\frac{1}{q_t^2} = \frac{1}{q_0^2} + K_3 t \quad (26)$$

Where q_t^2 is the amount of pollutant removed at time t (mg/g), q_o is the amount of solute sorbed at time t = 0 (mg/g), and K_3 second-order rate constant (g/mg min). The plot of 1 / q_t^2 against t gives a straight line, and the values for K_3 and q_o can be calculated from the slope and intercept, respectively (10).

2.8.7. Fractional power model

The nonlinear and linear forms of the fractional power kinetic model equation are depicted in equations 27-28;

$$q_t = K t^v \quad (27)$$

$$\log q_t = \log K + v \log t \quad (28)$$

Where log K and v are the intercept and slope of the plot of log q_t against log t respectively. Thus, the antilog of intercept gives the value of constant K. v is also a constant that is usually less than unity if the adsorption kinetic data fits well into the power function model. q_t is the quantity of adsorbate adsorbed at time t (10).

2.9. Mass Transfer Diffusion

2.9.1. Weber-Morris' transfer diffusion

To predict the rate of determining steps in the adsorption process of the pollutants,

$$q_t = K_{wm} t^{0.5} + C \quad (29)$$

A graph of q_t against $t^{0.5}$ is plotted. Where K_{wm} (mg/gmin$^{0.5}$) is the intra-particle diffusion rate constant and C (mg/g) is proportional to the boundary layer thickness (10).

2.9.2. Dumwald-Wagner transfer diffusion

This is another form of the intra-particle model developed by Dumwald-Wagner. The Equation is given as:

$$\log\left(1 - F^2\right) = \frac{-K}{2.303} t \quad (30)$$

K is the diffusion rate constant, F is the adsorption capacity, and it is gotten as F = q_t/q_e, q_t is the adsorption capacity at each time and he is the adsorption capacity at equilibrium (10).

2.9.3. Matthew-Weber transfer diffusion

The model is used to examine the external mass transfer in the boundary phase around the solid particle. The equation is given as:

$$\log \frac{C_t}{C_e} = \frac{-Km.A}{2.303} . t \quad (31)$$

Indicating a plot of log C_t/C_o against t, where C_t and C_o are the adsorbate concentration at time t and the initial solute concentration, mg/g, K_m is the external mass transfer coefficient m/h and A is the external surface per unit mass, m^2/g (10).

2.9.4. Banghams transfer diffusion

This model is employed to determine if the rate-limiting step is controlled by pore diffusion alone or not.

$$\log\left(\log\frac{Co}{Co-q_t.m}\right)=\log\left(\frac{K_b.m}{2.303.V}\right)+\theta logt \quad (32)$$

A graph of $\log\left(\log\frac{Co}{Co-q_t.m}\right)$ against log t, where V is the volume of the liquid phase, mL, is the weight of adsorbent per liter of solution g/L, and K_g and θ < 1 are constants (10).

2.9.5. McKay Film transfer diffusion

This involves mass transfer, which is based on film diffusion. It is represented as

$$\ln(1-F)=-K_m t \quad (33)$$

Where a graph of ln(1-F) is plotted against time to obtain K_m as the slope (16).

2.9.6. Vermeulin transfer diffusion

If the adsorbate diffusion through the adsorbent beads is the slowest step, the particle diffusion will be the rate-determining step. The expression of the model is as follows:

$$-\ln\left(1-\left(\frac{q_t}{q_e}\right)^2\right)=\left(\frac{2\pi^2 Dv}{r_0^2}\right)-Kv\cdot t \quad (34)$$

A plot of $-\ln\left(1-\left(\frac{q_t}{q_e}\right)^2\right)$ against time is made, where Dv is the effective diffusion coefficient, r_0^2 is the radius of the adsorbent particles supposed to be spherical particles, q_t / q_e is the fraction realization of equilibrium at a time, t (16).

2.9.7. Film transfer diffusion

The film diffusion model is represented as follows:

$$\log(q_m-q_t)=\log(q_m)-\frac{R}{2.303}t \quad (35)$$

Equation (35) has a similar structure to condition (20), showing that separating between film dissemination control and pseudo-first-order response control will be troublesome. Notwithstanding, doing a progression of sorption at various agitation speeds, as a rule, shows that film dissemination has a lot more grounded reliance on unsettling. In agitated sorption studies, film dispersion is generally just rate-controlling for an initial couple of moments (16).

3. RESULTS AND DISCUSSION

3.1. Characterization of Adsorbents

3.1.1. Morphological Characteristics of the adsorbent Using Scanning Electron Microscopy (SEM)

The scanning electron micrographs of the adsorbent were done before and after adsorption and are presented in Figures 1a-c and 2a-c, respectively. The SEM images indicate the surface area and pore spaces on the adsorbent, as shown in Figure 1a-c. TDX has more surface area and larger pore sizes. This showed that the TDX was viable in making well-developed pores on the outer layer of the antecedent for maximum adsorption, prompting TDX to have a huge surface region and permeable structure. The surface morphology of all the sorbents changed significantly by disturbing the pore spaces. It was identified that MB had been adsorbed onto the pores of the adsorbents, as shown in Figure 2a-c.

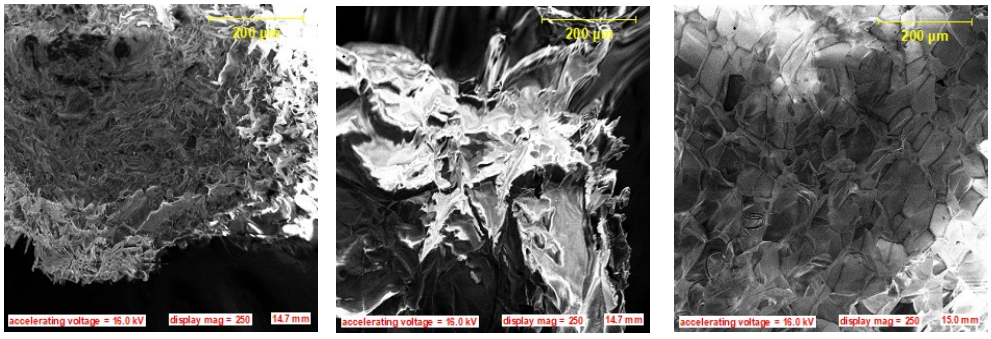

Figure 1: The morphology characteristics of adsorbent before adsorption (a) SEM Image of EPS(b) SEM Image of styrofoam (c) SEM Image of TDX.

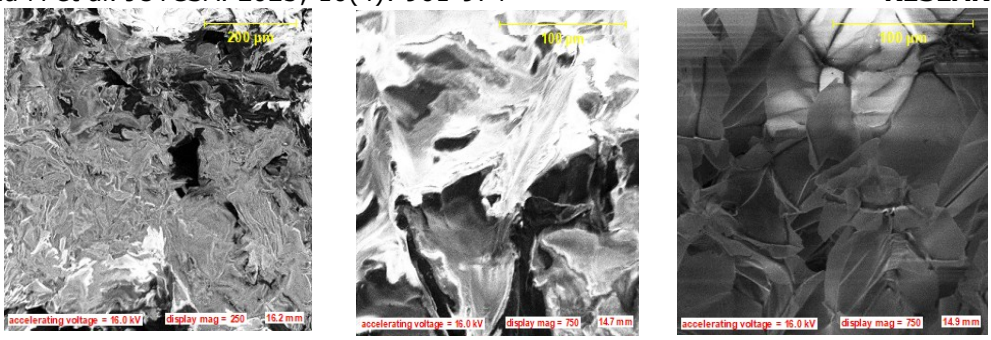

Figure 2: The morphology characteristics of adsorbent after adsorption (a) SEM Image of EPS(b) SEM Image of styrofoam (c) SEM Image of TDX.

3.2. Optimization of Concentration and Contact Time

The impact of concentration and contact time significantly affects the adsorption cycle, as displayed in Figures 3a-b. The impact of initial MB concentration in the range of 40 and 100 mg/L on adsorption was examined and is displayed in Figure 3a. It is clear from the figure that the level of MB removal diminished with the increase in the initial concentration of MB. The initial MB concentration gives the vital impetus to defeat the resistance to the mass transfer of MB between the fluid stage and the solid stage. The increase in initial MB concentration additionally improves the interaction between the material and MB. Hence, an increase in the initial MB concentration improves the adsorption take-up of MB. This is because of an increase in the driving force of the concentration gradient and an increase in the initial MB concentration. While the percentage of MB removal was found as 96.39% for 40 mg/L and 92.70% for 100 mg/L at 100 minutes. In addition, it was likewise seen that the pace of MB take-up increased rapidly in the initial 10 minutes of contact time. After around 10 minutes, the rate diminished for an additional 10 minutes until a steady MB focus was reached, this happened after around 80 minutes (Figure 3b). It was assumed that this time addressed the equilibrium time at which equilibrium MMB concentration occurred. This agrees with the result obtained by (5-7, 17).

The outcome can additionally be explained as follows, at first, the adsorption sites on the adsorbent were open, and MB cooperated effectively with the site. The concentration difference between the bulk solution and the solid-liquid interface was at first higher, which prompted the higher pace of adsorption after 10 minutes. A while later, MB was accumulated on the enormously accessible surface of adsorption sites on the adsorbent, which prompted the control of surface binding sites, dialing back adsorption. The graph affirmed the possibility of stopping the batch adsorption study at 80 min to optimize time for further study.

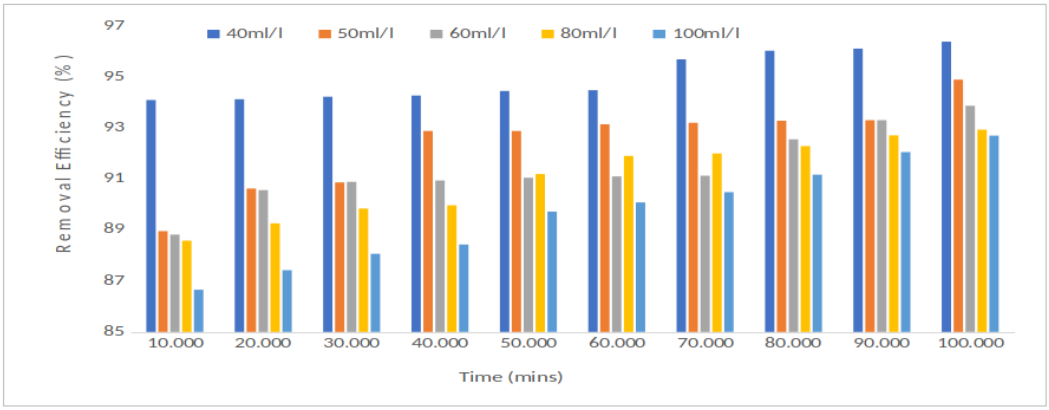

Figure 3a: Effect of contact time and concentration on removal efficiency.

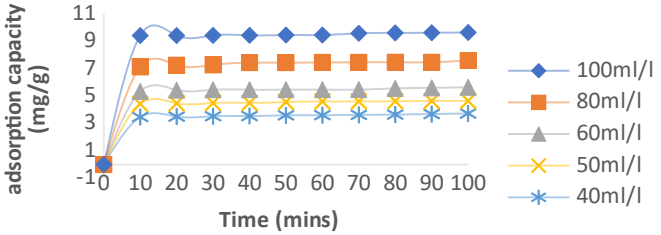

Figure 3b: Effect of contact time and concentration on adsorption capacity.

3.3. Adsorption Isotherm

Adsorption isotherm models can portray the cooperation between the adsorbate and adsorbent. This is an important criterion for optimizing the use of adsorbents. Eleven adsorption isotherms were studied in the investigation of the adsorption experiments. Langmuir 1-4, Freundlich, Temkin, Harkin-Jura, Hill-DeBoer, Dubinin-Radushkevich, Halsey, and Jovanovich were the isotherms selected because the values of their R^2 are greater than 0.9.

3.3.1. Langmuir model

The plots of Langmuir-1, Langmuir-2, Langmuir-3, and Langmuir-4 models were shown in Figure 4 which provided a linear relationship from which are $q_m \Lambda K_a$ determined from the slope and intercept of the plot. The q_m values for the contact time of Langmuir-1, Langmuir-2, Langmuir-3, and Langmuir-4 models were -17.0358, 13.4953, 7.9025, and -15.2446 respectively. The K_a parameters estimated are -0.0341, 0.0407, 0.0582, and -0.0372 for Langmuir-1, Langmuir-2, Langmuir-3, and Langmuir-4 Models, respectively. The correcting coefficient (R^2) for the Langmuir-1, Langmuir-2, Langmuir-3, and Langmuir-4 models was found to be 0.4344, 0.9155, 0.6385, and 0.6385, respectively. The R^2 value of Langmuir-2, which is highly significant than Langmuir-1, Langmuir-3, and Langmuir-4.

The negative values of some of the parameters show that the Langmuir model cannot be fitted, as the adsorption behavior does not follow the assumption on which the model is based (18), which shows that Langmuir isotherms 2 and 3 are more favorable for the treatment of MB in aqueous solution using polymeric adsorbent. The separation factor R can also be used to describe the essential characteristics of Langmuir. The value of R indicates the nature of the absorption process and the shape of the isotherm is irreversible (R = 0), favorable (0 < R> 1), linear (R = 1), or unfavorable (R >1) (12). The overall trend obtained for the R was all below one for all the concentration ranges studied, representing favorable adsorption processes. This showed good linearity for the Langmuir isotherm, which makes the isotherm valid and supports its applicability. The findings of the current study compare well with others reported in the literature (17, 19, 20).

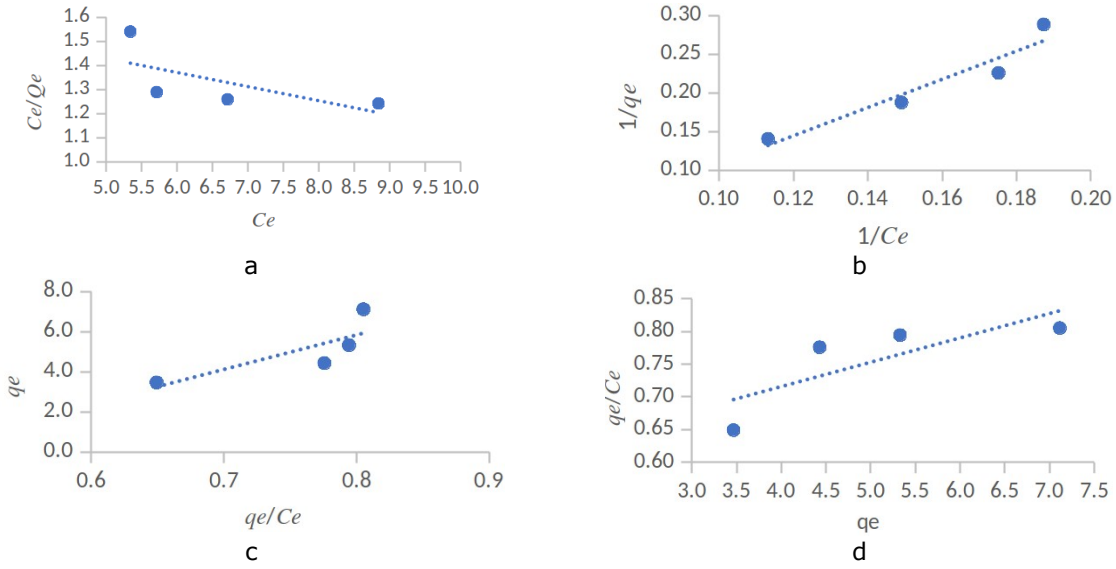

Figure 4: (a) Langmuir 1, (b) Langmuir 2, (c) Langmuir 3 and (d) Langmuir 4 Isotherms.

3.3.2. Freundlich model

The plot of $\ln q_e$ against $\ln C_e$ (Figure 5a provides a linear relationship from which $1/n$ and log K_f is gotten from the slope and intercept of the plot. The K_f value for the contact time of the Freundlich model was found to be 0.4172. The n parameter was also found to be 0.7603 and 1/n was estimated to be 1.3152. The R^2 for Freundlich's model is found to be 0.945. The R^2 value of the Freundlich model is highly significant. The absence of negative values indicates that the Freundlich isotherm can be used. Based on the correlation coefficients, the applicability of the isotherms was compared, and it showed that the Freundlich isotherm was a better fit for the adsorption data than the Langmuir isotherm. The surface heterogeneity of an adsorbent is addressed by utilizing the 1/n value, in which the adsorption is viewed as great and heterogeneous when the value of 1/n lies somewhere in the range of 0 and 1, the adsorption is homogenous in which there is no cooperation among the adsorbed species when 1/n = 1 and the adsorption is unfavorable when 1/n > 1.46. In this situation, the value of 1/n is under 1.46, and the adsorption is good for the Freundlich isotherm. The findings of the current study compare well with others reported in the literature (21).

3.3.3. Temkin model

The plot of $1-(C_e/C_o)$ against $\ln C_e$ (Figure 5b provides a linear relationship from which $RT/\Delta Q$ and $RT/\Delta Q \ln K_o C_e$ are determined from the slope and

intercept of the plot. The ΔQ value for a contact time was 0.0028. The estimated K parameter is 953.37. The Temkin Model R^2 is estimated as 0.9818. The R^2 value of the Temkin model is highly significant. While comparing the results with Langmuir and Freundlich, the Temkin isotherm model also shown that the R^2 values are close to unity. The findings of the current study compare well with others reported in the literature (22, 23).

3.3.4. Harkin-Jura model

The plot of $1 / q_e^b$ against $\log C_e$, (Figure, 5c) provides a linear relationship from which A and B are determined from the slope and intercept of the plot. The A value for a contact time is 3.9968. The q_o parameter is estimated as 1.0032. The R^2 of the Harkin-Jura model is 0.8062. The R^2 value is highly significant. Based on R^2 values of these isotherm models, it was concluded that the Freundlich, Jovanovich, Dubinin–Radushkevich, Temkin isotherms, and Langmuir 1,2 were better models than the Harkin-Jura model, however, Harkin-Jura constant, A values greater than 1, suggest better curve fitting, and the adsorption is favorable for Harkin-Jura isotherm (12, 21).

3.3.5. Hill-De Boer model

The plot of $\ln\left(\frac{Ce^2}{C_o - C_e\, e}\right) - \frac{C_o - C_e}{C_e}$ against $\frac{C_o - C_e}{C_o}$ (Figure 5d) provides a linear relationship from which $-K_2 / RT$ and $-\ln K_1$ is determined from the slope and intercept of the plot. The K_2 value for a contact time is 1553374.67. The K_1 parameter estimated is 4.18E-23. The R^2 for Hill-De Boer model is 0.9566, which is highly significant. The R^2 value of the Hill-De Boer Model is highly significant. While comparing the results with Langmuir, Freundlich, Jovanovich, Dubinin–Radushkevich, and Hill-De Boer isotherm models, it was seen that the R^2 values are closer to unity.

3.3.6. Halsey model

The plot of $\ln q_e$ against $\ln C_e$ (Figure 5e) provides a linear relationship from which $-1 / nH$ and $\ln K_H$ is determined from the slope and intercept of the plot. The n_H value for a contact time is -0.7603. The K_H parameter was estimated as 1.9439. The Halsey Model R^2 was found to be 0.945. The R^2 value is highly significant. The findings of the current study compare well with others reported in the literature (21).

3.3.7. Dubinin Radushkevich model

The plot of $\ln q_e$ against ε^2 (Figure 5f) provides a linear relationship from which ß and $\ln q_m$ are determined from the slope and intercept of the plot. The ß value for contact time is -6E-06. The q_m parameter was estimated as 11.0851. The R^2 for Dubinin Radushkevich model is estimated as 0.975. The R^2 value is highly significant. The findings of the current study compare well with others reported in the literature (24).

3.3.8. Jovanovich model

The plot of $\ln q_e$ against C_e (Figure 5g) provides a linear relationship from which K_f and q_{max} are determined from the slope and intercept of the plot. The K_f value for contact time is 0.1853. The q_{max} parameter is estimated as 1.4329. The R^2 for Jovanovich model is 0.9191. The R^2 value is highly significant. The Jovanovich equilibrium constant Kj was almost the same as the values reported by (7).

3.3.9. Selection of suitable isotherm

The fitness of the isotherms to the data obtained from the study was analyzed based on the R^2, and the Temkin isotherm model has the highest value (0.9818) while Langmuir 3 has the least (0.6385). The sequence of the suitability of the isotherms based on average is Temkin > Dubinin > Hill-De > Halsey > Freundlich > Jovanovich > Langmuir -2 > Harkin-J > Langmuir -3, as shown in Table 1. Langmuir 1 and 4 were exempted because some of their isotherm parameters were negative and could not be used to describe the adsorption process.

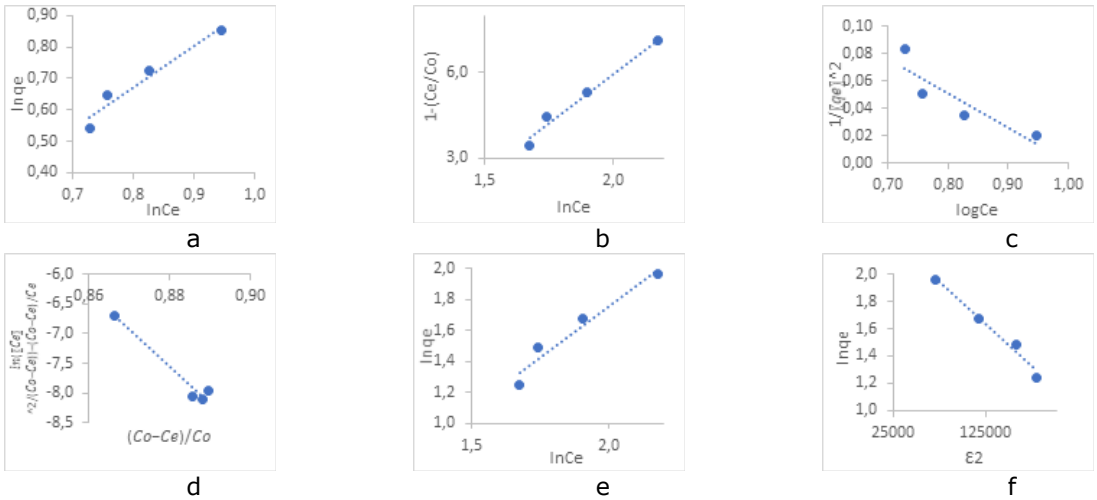

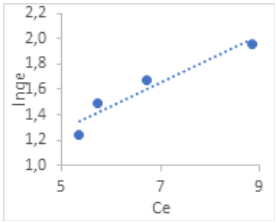

g

Figure 5: Model isotherms. (a) Freundlich, (b) Temkin, (c) Harkin-Jura, (d) Hill-De Boer, (e) Halsey, (f) Dubinin Radushkevich, and (g) Jovanovich.

Table 1: Suitable isotherm models.

Model	(R^2)	Model	(R^2)
Langmuir-1	0.4344	Temkin	0.9818
Langmuir-2	0.9155	Harkin- Jura	0.8062
Langmuir-3	0.6385	Hill-De Boer	0.9566
Langmuir-4	0.6385	Halsey	0.945
Freundlich	0.945	D-R	0.975

3.4. Kinetic Studies for Different Concentrations

3.4.1. Zero Order

The plot of q_t^* against t (Figure 6a) provides a linear relationship from which K_o and q_o^* are determined from the slope and intercept of the plot, as seen in Table 2. The K_o values for the contact time of MB at different concentration ranges of 100, 80, 60, 50, and 40 mg/L were 0.0029, 0.0042, 0.0027, 0.0025, and 0.0027, respectively. The q_o^* parameters estimated at 100, 80, 60, 50 and 40 mg/L are 9.3395, 7.1641, 5.3381, 4.416, and 3.4386 mg/g, respectively. These values were lower compared to their corresponding qe experimental values (9.6390, 7.5919, 5.6323, 4.6467, and 3.7241 mg/g respectively). The R^2 values are 0.8689, 0.8254, 0.8558, 0.9600, and 0.9889, respectively. The highest value of R^2 is 0.9889 at 40 mg/L. In addition, it was observed that only R^2 at 40 mg/L is not far from unity, and this implies that a Zeroth order kinetic model can be used to fit the adsorption of MB only for 40 mg/L and is not suitable for higher concentrations.

3.4.2. First Order

The plot of log (q_m-q_t) against t (Figure 6b) provides a linear relationship from which K_1 and q_m are determined from the slope and intercept of the plot. The K_1 values for a contact time of MB at different concentration ranges of 100, 80, 60, 50, and 40 mg/L were 0.0003, 0.0006, 0.0005, 0.0005, and 0.0008, respectively. The q_o^* parameters estimated at 100, 80, 60, 50 and 40 mg/L are 9.3409, 7.1657, 5.3393, 4.4172, and 3.4408 mg/g, respectively. These values, just like zeroth order, were also lower compared to their corresponding q_e experimental values, which were 9.6390, 7.5919, 5.6323, 4.6467, and 3.7241 mg/g, respectively, for 100, 80, 60, 50, and 40 mg/L concentration. The R^2 for 100, 80, 60, 50 and 40 mg/L are 0.8689, 0.8253, 0.8556, 0.9585, and 0.9896, respectively. The highest value of R^2 is 0.9896 at 40 mg/L. In addition, it was observed that only R^2 at 40 mg/L is not far from unity, and this implies that the first-order kinetic model can also be used to fit the adsorption of MB only at 40 mg/L and is not suitable for higher concentrations.

3.4.3. Pseudo-first Order

The plot of ln(q_e-q_t) against t (Figure 6c) provides a linear relationship from which K_1 and $lnq_{e(cal.)}$ are determined from the slope and intercept of the plot. The K_1 values for a contact time of MB at different concentration ranges of 100, 80, 60, 50, and 40 mg/L were -0.0029, -0.0042, -0.0027, -0.0025, and -0.0027, respectively. The q_e parameters estimated at 100, 80, 60, 50, and 40 mg/L are 1.3487, 1.5338, 1.3421, 1.2596, and 1.3306, respectively. These values were lower compared to Zero and first order and also to their corresponding q_e experimental values, which were 9.6390, 7.5919, 5.6323, 4.6467, and 3.7241 mg/g, respectively, for 100, 80, 60, 50, and 40 mg/L concentrations. The R^2 for 100, 80, 60, 50 and 40 mg/L are 0.8689, 0.8254, 0.8558, 0.96, and 0.9889, respectively. The highest value of R^2 is 0.9889 at 40 mg/L. In addition, it was observed that only R^2 at 40 mg/L is not far from unity, and this implies that a Zeroth order kinetic model can be used to fit the adsorption of MB only for 40 mg/L and is not suitable for higher concentrations.

3.4.4. Second Order

The plot of 1 / q_t against t (Figure 6d) provides a linear relationship from which K_2 and q_o are determined from the slope and intercept of the plot. The K_1 values for a contact time of MB at different concentration ranges of 100, 80, 60, 50, and 40 mg/L were -0.0003, -0.0008, -0.0009, -0.0001, and -0.0002, respectively. The q_e parameters estimated at (100, 80, 60, 50 and 40 mg/L are 9.3457, 7.1684, 5.3418, 4.4189, and 3.4435, respectively. These values just like other kinetic models were also lower compared to their corresponding q_e experimental which were 9.6390, 7.5919, 5.6323, 4.6467, and 3.7241 mg/g, respectively, for 100, 80, 60, 50, and 40 mg/L concentrations. The R^2 for 100,

80, 60, 50, and 40 mg/L concentrations are 0.9999, 0.9998, 0.9996, 0.9999, and 0.9995, respectively, which were very close to unity and further made the model a better fit than the zeroth, first-order, and pseudo-first-order kinetics models. Thus, it was presumed that the second-order model provides a better correlation of adsorption fit than the zeroth, first-order, and pseudo-first-order models.

3.4.5. Pseudo-second Order

The plot of 1 / q_t against t (Figure 6e) provides a linear relationship from which K_2 and q_o are determined from the slope and intercept of the plot. The K_1 values for a contact time of MB at different concentration ranges of 100, 80, 60, 50, and 40 mg/L were -0.0003, -0.0008, -0.0009, -0.0001, and -0.0002, respectively. The q_e parameters estimated at 100, 80, 60, 50, and 40 mg/L are 9.3457, 7.1685, 5.3418, 4.4189, and 3.4435 mg/g, respectively. These values just like other kinetic models were also lower compared to their corresponding q_e experimental values, which were 9.6390, 7.5919, 5.6323, 4.6467, and 3.7241 mg/g, respectively, for 100, 80, 60, 50, and 40 mg/L concentrations. The R^2 for 100, 80, 60, 50, and 40 mg/L concentrations are 0.9999, 0.9998, 0.9996, 0.9999, and 0.9995, respectively, which were very close to unity and further made the model a better fit than the zeroth, first-order, pseudo-first-order, and second-order kinetics model. Thus, it was presumed that the pseudo-second-order provides a better correlation of adsorption fit than the zeroth, first-order, pseudo-first-order, and second-order. The results also indicate that the adsorption of MB was consistent with a pseudo-second-order kinetic equation and that its adsorption was mainly via chemisorption.

3.4.6. Third Order

The plot of 1 / q_t^2 against t (Figure 6f) provides a linear relationship from which K_3 and q_o are determined from the slope and intercept of the plot. The K_1 values for a contact time of MB at different concentration ranges of 100, 80, 60, 50, and 40 mg/L were -7E-06, -0.00002, -0.00003, -0.00005, and -0.00001, respectively. The q_e parameters estimated at 100, 80, 60, 50, and 40 mg/L are 9.3250, 7.1611, 5.3452, 4.4194, and 3.4442, respectively. These values just like other kinetic models were also lower compared to their corresponding q_e experimental values, which were 9.6390, 7.5919, 5.6323, 4.6467, and 3.7241 mg/g respectively for 100, 80, 60, 50, and 40 mg/L concentration. The R^2 for 100, 80, 60, 50, and 40 mg/L are 0.8705, 0.8157, 0.8545, 0.9555, and 0.9902, respectively. The highest value of R^2 is 0.9902 at 40 mg/L. In addition, it was observed that only R^2 at 40 mg/L is not far from unity, and this implies that the third-order kinetic model can also be used to fit the adsorption of MB only at 40 mg/L and is not suitable for higher concentrations.

3.4.7. Selection of suitable isotherm

The suitability of the kinetic model to the data obtained from the study was analyzed based on the R^2, and it was observed that only R^2 at 40 mg/L is not far from unity zeroth, first-order, pseudo-first-order, third-order, and this implies that these kinetic models can also be used to fit the adsorption of MB only at 40 mg/L and are not suitable for higher concentration. The R^2 for the second-order and pseudo-second-order Kinetic models were very close to unity at all concentrations, which further made the model a better fit than the zeroth, first-order, and pseudo-first-order kinetic models. Thus, it was presumed that the second-order and pseudo-second-order Kinetic models provide a better correlation of adsorption fit than the zeroth, first-order, and pseudo-first-order models. The results also indicate that the adsorption of MB was consistent with a pseudo-second-order kinetic equation, and that its adsorption was mainly via chemisorption.

Table 2: Kinetic Models for Effect of Concentration.

Concentration		100 ml/L	80 ml/L	60 ml/L	50 ml/L	40 ml/L
Zeroth Order	$q_{e(exp)}$	9.639	7.5919	5.6322	4.6467	3.7242
	q_o	9.339	7.1641	5.3381	4.4160	3.4386
	K_o	0.0029	0.0042	0.0027	0.0025	0.0027
	R^2	0.8689	0.8254	0.8558	0.9600	0.9889
First Order	q_o	9.3408	7.1656	5.3393	4.4172	3.4408
	K_1	0.0003	0.0006	0.0005	0.0005	0.0008
	R^2	0.8694	0.8223	0.8556	0.9585	0.9896
Pseudo-First Order	q_o	1.3487	1.5338	1.3420	1.2596	1.3306
	K_1	-0.0029	-0.0042	-0.0027	-0.0025	-0.0027
	R^2	0.8689	0.8254	0.8558	0.9600	0.9889
Second Order	q_o	9.3457	7.1685	5.3418	4.4189	3.4435
	K_2	-0.00003	-0.00008	-0.00009	-0.0001	-0.0002
	R^2	0.87	0.8191	0.8552	0.9571	0.9900
Pseudo-Second Order	q_o	9.6805	7.5930	5.6433	4.6838	3.7439
	K_2	0.1312	0.1274	0.1510	0.1897	0.1519
	R^2	0.9999	0.9998	0.9996	0.9999	0.9995
Third Order	q_o	9.3251	7.1611	5.3452	4.4194	3.4442
	K_3	-7E-06	-0.00002	-0.00003	-0.00005	-0.0001
	R^2	0.8705	0.8157	0.8545	0.9555	0.9902

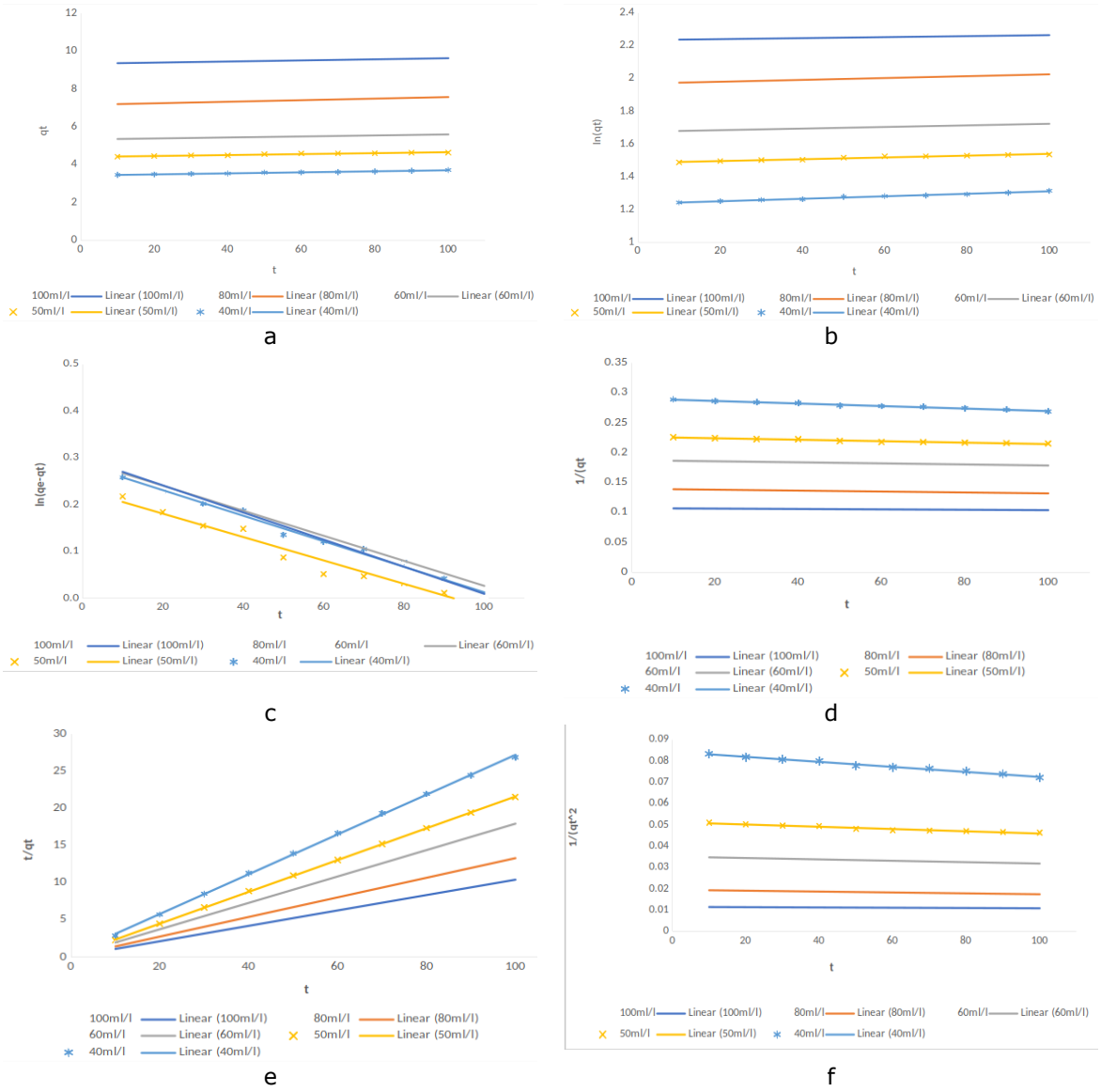

Figure 6: (a) Zeroth Order Kinetic Model, (b) First Order Kinetic Model (c): Pseudo-First Order Kinetic Model (d) Second-Order Kinetic Model (e) Pseudo-Second Order Kinetic Model, and (f) Third Order Kinetic Model.

3.5. Mass Transfer for Diffusion for Effect of Concentration Model

3.5.1. Webber-Morris Mass Transfer

The plot q_e against $t^{1/2}$ (Figure 7a) describes the relationship between the Weber Morris constant as obtained from the slope and intercept of the plot. The intraparticle diffusion parameters obtained from the plot are C_{wm} and R^2. Where k_{ami} is the slope and C is the intercept. The k_{wm} values for a contact time of MB at different concentration ranges of 100, 80, 60, 50, and 40 mg/L were 0.0372, 0.0582, 0.037, 0.034, and 0.0364 mg/g/min$^{0.5}$, respectively, which is less than 0.1 mg/g/min$^{0.5}$, which clearly show that adsorption stages did not occur in multiples (16). The R^2 for 100, 80, 60, 50, and 40 mg/L are 0.7841, 0.8896, 0.8327, 0.9731, and 0.9616, respectively. The highest value of R^2 is 0.9731, which is close to unity, suggesting that the adsorption process was surface diffusion dominant and showed a good fit to the experimental data.

3.5.2. McKay

The plot ln (1-F) against t (Figure 7b) describes the relationship between the McKay constant as obtained from the slope of the plot. The k values for a contact time of MB at different concentration ranges of 100, 80, 60, 50, and 40 mg/L were -0.0119, -0.0073, -0.0085, -0.0148, and -0.0089, respectively. The R^2 for 100, 80, 60, 50, and 40 mg/L are 0.7632, 0.8327, 0.706, 0.9208 and 0.923, respectively. The highest value of R^2 is 0.923 at 40 mg/L. The negative value of km and fluctuation of values of R^2 as concentration increased showed a trend that could be derived as not being a good function of concentrations.

3.5.3. Dumwald Wagner

The plot log (1-F^2) against t (Figure 7c), describes the relationship between the Dumwald Wagner

constants. The intraparticle diffusion parameters K and R^2 are evaluated from the plot. The k values for a contact time of MB at different concentration ranges of 100, 80, 60, 50, and 40 mg/L were 0.02718, 0.01658, 0.01935, 0.03385, and 0.02004, respectively. The R^2 for 100, 80, 60, 50, and 40 mg/L are 0.7628, 0.8336, 0.7041, 0.9194, and 0.9208, respectively. The highest value of R^2 is 0.9208 at 40 mg/L.

3.5.4. Vermeulin

The plot $-\ln(q_t/q_e)^2$ against t (Figure 7d) describes the relationship between the Verneulin constants. The diffusion parameters K_V, D_V, and R^2 are evaluated from the plot. The K_V values for a contact time of MB at different concentration ranges of 100, 80, 60, 50 and 40 mg/L were -2.72E-02, -1.65E-02, -1.94E-02, -3.39E-02, and -2.00E-02, respectively, and the estimated D_V values for contact time of MB at different concentrations ranges of 100, 80, 60, 50, and 40 mg/L were 1.4813, 1.3712, 1.2952, 1.1191, and 1.0592, respectively. The R^2 for 100, 80, 60, 50, and 40 mg/L are 0.7628, 0.8336, 0.7041, 0.9194, and 0.9208, respectively. The highest value of R^2 is 0.9208 at 40 mg/L.

3.5.5. Film Transfer

The plot $\log(q_m - q_t)$ against t (Figure 7e) describes the relationship between the film transfer constants R* and q_m as obtained from the slope and intercept of the plot. The diffusion parameters R*, q_m, and R^2 are derived from the plot. The R* values for a contact time of MB at different concentration ranges of 100, 80, 60, 50, and 40 mg/L were 0.027406, -0.0073, -0.0085, -0.0148, and -0.0089, respectively, and the estimated q_m values for a contact time of MB at the different concentration range of 100, 80, 60, 50, and 40 mg/L were 0.4783, 0.453524, 0.378181, 0.411339, and 0.36686, respectively. The R^2 for 100, 80, 60, 50, and 40 mg/L are 0.7632, 0.8327, 0.706, 0.9208, and 0.923, respectively. The highest value of R^2 is 0.923 at 40 mg/L.

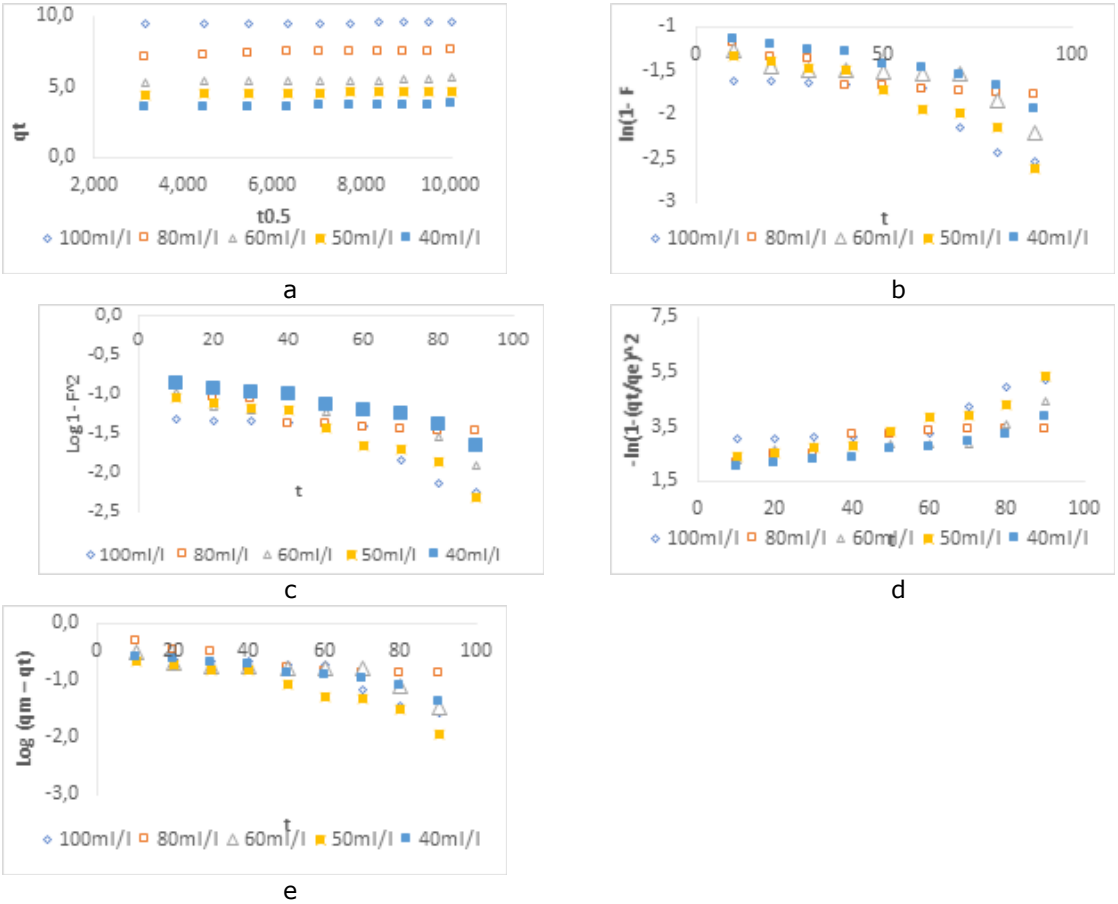

Figure 7: (a) Webber- Morris Mass Transfer, (b) McKay Mass Transfer (c) Dumwald-Wagner Mass Transfer (d) Vermeulin, and (e) Film Mass Transfer.

4. CONCLUSION

The polymeric waste was successfully chemically recycled into the novel functional adsorbent composite. The synthesized adsorbent composite was applied for the treatment of MB wastewater. The adsorption capacity and removal efficiency showed a linear relationship between the investigated entities, concentration, and contact time. The result also showed that adsorption capacity and removal efficiency increase as concentration and contact time increase. The equilibrium data shows that Langmuir, Freundlich, Temkin, Harkin-J, Hill-De, Dubinin, Halsey, and

Jovanovich isotherms are more suitable for MB removal because the values of their R^2 are greater than 0.9. It can be deduced that the order of isotherms fit for MB is as follows; Temkin > Dubinin > Hill-De > Halsey > Freundlich > Jovanovich > Langmuir -2 > Harkin-J > Langmuir -4> Langmuir -3 > Langmuir -1. The kinetic model that best describes the adsorption of MB onto the polymeric composite produced is the pseudo-second-order model. The Weber- Morris Mass Transfer has the highest value of R^2 and is the most suitable model for the adsorption of MB onto the polymeric composite.

5. REFERENCES

1. Bekri-Abbes I, Bayoudh S, Baklouti M. Converting Waste Polystyrene into Adsorbent: Potential Use in the Removal of Lead and Cadmium Ions from Aqueous Solution. J Polym Environ [Internet]. 2006 Nov 21;14(3):249–56. Available from: <URL>.

2. Pan B, Pan B, Zhang W, Lv L, Zhang Q, Zheng S. Development of polymeric and polymer-based hybrid adsorbents for pollutants removal from waters. Chem Eng J [Internet]. 2009 Aug 15;151(1–3):19–29. Available from: <URL>.

3. Parashar N, Hait S. Plastics in the time of COVID-19 pandemic: Protector or polluter? Sci Total Environ [Internet]. 2021 Mar 10;759:144274. Available from: <URL>.

4. Santoso E, Ediati R, Kusumawati Y, Bahruji H, Sulistiono DO, Prasetyoko D. Review on recent advances of carbon based adsorbent for methylene blue removal from waste water. Mater Today Chem [Internet]. 2020 Jun 1;16:100233. Available from: <URL>.

5. N'diaye AD, Aoulad El Hadj Ali Y, Bollahi MA, Stitou M, Kankou M, Fahmi D. Adsorption of Methylene Blue from aqueous solution using Senegal River Typha australis. Mediterr J Chem [Internet]. 2020 Jan 22;10(1):22–32. Available from: <URL>.

6. Song J, Zou W, Bian Y, Su F, Han R. Adsorption characteristics of methylene blue by peanut husk in batch and column modes. Desalination [Internet]. 2011 Jan 15;265(1–3):119–25. Available from: <URL>.

7. Alade AO, Amuda OS, Afolabi TJ, Okoya AA. Adsorption of naphthalene onto activated carbons derived from milk bush kernel shell and flamboyant pod. J Environ Chem Ecotoxicol [Internet]. 2012 Apr 2;4(7):124–32. Available from: <URL>.

8. Ge M, Wang X, Du M, Liang G, Hu G, S.M. JA. Adsorption Analyses of Phenol from Aqueous Solutions Using Magadiite Modified with Organo-Functional Groups: Kinetic and Equilibrium Studies. Materials (Basel) [Internet]. 2018 Dec 28;12(1):96. Available from: <URL>.

9. Langmuir I. The Constitution and Fundamental Properties of Solids and Liquids. Part I. Solids. J Am Chem Soc [Internet]. 1916 Nov 1;38(11):2221–95. Available from: <URL>.

10. Unuabonah EI, Omorogie MO, Oladoja NA. Modeling in Adsorption: Fundamentals and Applications. In: Composite Nanoadsorbents [Internet]. Elsevier; 2019. p. 85–118. Available from: <URL>.

11. Hall KR, Eagleton LC, Acrivos A, Vermeulen T. Pore- and Solid-Diffusion Kinetics in Fixed-Bed Adsorption under Constant-Pattern Conditions. Ind Eng Chem Fundam [Internet]. 1966 May 1;5(2):212–23. Available from: <URL>.

12. Alam MS, Khanom R, Rahman MA. Removal of Congo Red Dye from Industrial Wastewater by Untreated Sawdust. Am J Environ Prot [Internet]. 2015 [cited 2023 Aug 29];4(5):207–13. Available from: <URL>.

13. Freundlich H. Über die Adsorption in Lösungen. Zeitschrift für Phys Chemie [Internet]. 1907 Oct 1;57U(1):385–470. Available from: <URL>.

14. Hutson ND, Yang RT. Theoretical basis for the Dubinin-Radushkevitch (D-R) adsorption isotherm equation. Adsorption [Internet]. 1997 Sep;3(3):189–95. Available from: <URL>.

15. Li Y-H, Wang S, Luan Z, Ding J, Xu C, Wu D. Adsorption of cadmium(II) from aqueous solution by surface oxidized carbon nanotubes. Carbon N Y [Internet]. 2003 Jan 1;41(5):1057–62. Available from: <URL>.

16. Dada AO, Latona DF, Ojediran OJ, Nath OO. Adsorption of Cu (II) onto bamboo supported manganese (BS-Mn) nanocomposite: effect of operational parameters, kinetic, isotherms, and thermodynamic studies. J Appl Sci Environ Manag [Internet]. 2016 Jul 25;20(2):409–22. Available from: <URL>.

17. Kadhom M, Albayati N, Alalwan H, Al-Furaiji M. Removal of dyes by agricultural waste. Sustain Chem Pharm [Internet]. 2020 Jun 1;16:100259. Available from: <URL>.

18. Priyadarshini B, Rath PP, Behera SS, Panda SR, Sahoo TR, Parhi PK. Kinetics, Thermodynamics and Isotherm studies on Adsorption of Eriochrome Black-T from aqueous solution using Rutile TiO 2. IOP Conf Ser Mater Sci Eng [Internet]. 2018 Feb 1;310(1):012051. Available from: <URL>.

19. Boukhemkhem A, Rida K. Improvement adsorption capacity of methylene blue onto modified Tamazert kaolin. Adsorpt Sci Technol [Internet]. 2017 Dec 25;35(9–10):753–73. Available from: <URL>.

20. Ozudogru Y, Merdivan M, Göksan T. Biosorption of Methylene Blue fromAqueous Solutions by Iron Oxide-Coated Cystoseira barbata. J Turkish Chem Soc Sect A Chem [Internet]. 2016 Oct 5;3(3):551–64. Available from: <URL>.

21. Babalola BM, Babalola AO, Akintayo CO, Lawal OS, Abimbade SF, Oseghe EO, et al. Adsorption and desorption studies of Delonix regia pods and leaves: removal and recovery of Ni(II) and Cu(II) ions from aqueous solution. Drink Water Eng Sci [Internet]. 2020 Jul 17;13(2):15–27. Available from: <URL>.

22. Chandran V, Muthuraman P, Rajalekshmi G, Amrithaa TS, Viji Chandran S, Pandimadevi M. Preparation and characterisation of activated carbon from Delonix regia seeds for the removal of methylene blue dye. J Ind Pollut Control [Internet]. 2016;32(2):572–9. Available from: <URL>.

23. Dehghani MH, Tajik S, Panahi A, Khezri M, Zarei A, Heidarinejad Z, et al. Adsorptive removal of noxious cadmium from aqueous solutions using poly urea-formaldehyde: A novel polymer adsorbent. MethodsX [Internet]. 2018 Jan 1;5:1148–55. Available from: <URL>.

24. Amole AR, Araromi DO, Alade AO, Afolabi TJ, Adeyi VA. Biosorptive removal of nitrophenol from aqueous solution using ZnCl2-modified groundnut shell: optimization, equilibrium, kinetic, and thermodynamic studies. Int J Environ Sci Technol [Internet]. 2021 Jul 30;18(7):1859–76. Available from: <URL>.